Chemical Science

ROYAL SOCIETY OF CHEMISTRY

EDGE ARTICLE

View Article Online
View Journal | View Issue

Cite this: *Chem. Sci.*, 2022, **13**, 10315

All publication charges for this article have been paid for by the Royal Society of Chemistry

Received 29th May 2022
Accepted 8th August 2022

DOI: 10.1039/d2sc02986c

rsc.li/chemical-science

Phototriggered color modulation of perovskite nanoparticles for high density optical data storage†

Jie Chen, Zelian Xu, Jingcheng Zheng, Haishan Wu and Yuwu Chi *

Photoresponsive luminescent materials (PLMs) have attracted much attention in various optoelectronic fields, especially in optical data storage. Multi-wavelength (N-wavelength) based optical storage is a promising approach to increase the data storage density, but its current application is limited by the fact that most PLMs have only two-wavelength emissive states after certain light excitation, which requires simultaneous use of several PLMs and different irradiation light sources. In this study, we discovered that the wavelength of perovskite nanocrystals (PNCs) in the presence of dichloromethane (DCM) could be continuously and precisely tuned over a very wide color range (from red to violet) with the help of a single UV light source. The changes in crystal structures and optical properties of PNCs during UV irradiation were investigated in detail; the effects of capping ligand, solvent, UV irradiation power and time were evaluated, and the mechanism of UV triggered PNC fluorescence change was studied and is discussed. Finally, the applicability of PNCs/DCM film in N-wavelength-based high-density optical data storage was verified.

Introduction

Stimuli-responsive luminescent materials (SRLMs)[1–5] are a kind of smart materials[6] showing remarkable fluorescence change when exposed to external stimuli such as light,[7] temperature,[8] gas,[9] electrical potential,[10–12] and stress.[13,14] SRLMs have drawn much attention for their cutting-edge applications in displays,[15,16] sensors[17,18] and security protection like encryption of information.[19,20] Among SRLMs, photoresponsive luminescent materials (PLMs)[3–5] with several obvious advantages, such as non-invasiveness, accurate spatiotemporal operation of photostimulation and excellent photoresponsivity of the substrate,[21] have had extensive applications in the fields of optical control,[22–25] optical switching,[26–29] optical data recording and storage.[30–35]

Traditionally, organic PLMs have received a great deal of attention due to their advantages such as fast photoresponse, facile modification and color tunability.[36,37] However, the issue of complicated synthesis route, weak thermostability, and having few photoresponsive isomers limit their further practical applications.[38] As an alternative, inorganic PLMs with the advantages of superior long-term stability and facile preparation are considered to be good candidates for the next generation of high-density optical data storage and 3D graphics memory devices.[39–41]

Recently, perovskite nanocrystals (PNCs) have received great attention because of their brilliant photoelectric properties such as high fluorescence quantum yield (QY) and narrow full width at half-maximum (FWHM).[42–46] Especially, the tunable fluorescence covers the entire visible wavelength region,[47] which implies that PNCs may become a new type of responsive luminescent materials. Generally, the tuning of bandgap energy and fluorescence wavelength of PNCs is achieved by controlling the particle size[47] or halide composition.[48–50] Rather remarkably, compositional modulation by a simple ion exchange could readily tune the fluorescence spectrum of PNCs to cover the full visible spectrum ranging from 400 nm to 700 nm.[51] Unfortunately, the anion exchange reaction usually proceeds by dissolving the halide sources in polar solvents and subsequently adding them into purified PNC solutions, which would easily deteriorate the structure and weaken the fluorescence.[48,51] Therefore, it's critical to improve the colloidal stability by adopting a novel method to generate halide sources during the ion exchange process, rather than the tedious and intrusive addition of halide by hand operation.

In an innovative and non-invasive manner, light enables precise and remote control and spatiotemporal manipulation.[21] Particularly, computer-assisted Laser Direct Writing (LDW)[52,53] is an alternative method to sculpture various patterns with the merits of no mask requirement, easy operation, accurate programming, high-throughput and efficient fabrication. Furthermore, photo-irradiation could directly or catalytically decompose some materials,[54–56] for instance, dichloromethane (DCM) would spontaneously undergo dissociation to generate chlorine radicals upon UV irradiation.[57] Employing light as the

MOE Key Laboratory for Analytical Science of Food Safety and Biology, Fujian Provincial Key Laboratory for Food Safety and Detection, College of Chemistry, Fuzhou University, Fuzhou, 350108, P. R. China. E-mail: y.w.chi@fzu.edu.cn

† Electronic supplementary information (ESI) available: Fig. S1–S23. See https://doi.org/10.1039/d2sc02986c

switch of the anion-exchange reaction to avoid further damage of PNC structures induced by polar solvents might provide a non-invasive method for introducing halide sources. All of these cognitive processes suggest that PNCs may be qualified for the next-generation PLMs.

On an occasion, we discovered that PNCs in DCM could act as a good PLM. On the morning of a sunny winter day in 2019, warm sunshine from the southeast passed through a lab window and shone on a bottle of PNCs in DCM and a bottle of PNCs in toluene which were placed together on an experimental desk. Soon after, we found that PNCs in DCM changed their fluorescence from green to blue quickly, whereas PNCs in toluene had their green fluorescence unchanged. Later, it turned out that both DCM and oleylamine (OAm) played key roles in the photoresponsive luminescence variation. In this work, we develop a new type of PNC-based PLMs, in which OAm-PNCs (*i.e.* OAm as the sole capping ligand) are synthesized and used as the luminophores, and DCM acts both as the chlorine source and reaction medium (Scheme 1). The approach of photo-treatment of OAm-PNCs-DCM can accurately tune the successive shift of PL peaks within several nanometers, which is hard to access by roughly adding a stoichiometric reagent with manual operation (Scheme 1a). The fluorescence of the PNC-based PLMs can be tuned from green to blue by using OAm-$CsPbBr_3$ PNCs-DCM, and from red to green by using OAm-$CsPb(Br_{0.4}I_{0.6})_3$ PNCs-DCM, which enables the precise modulation of fluorescence over the whole visible light (from red to violet) domain by UV light stimuli. The mechanisms of photo-triggered dissociation of the chlorine anion (Cl^-) from DCM and alkylamine assisted ion exchanges were investigated and are discussed (Scheme 1b). Thanks to the satisfactory photo-triggered modulation of the fluorescence of OAm-PNCs-DCM, we therefore combined OAm-PNCs-DCM with a UV-curable resin (UCR) to make a facile PNC-based optical data memory (shown in Scheme 1c). Optical data information related to UV irradiation time or UV-laser scanning cycles can be precisely recorded by lithography of the PNCs-UCR-DCM film with colorful patterns. It is envisioned that the PNCs-DCM system with the merits of sensitive and fast photoresponse, wide and precise wavelength tunability may have promising applications in high-density optical data storage.

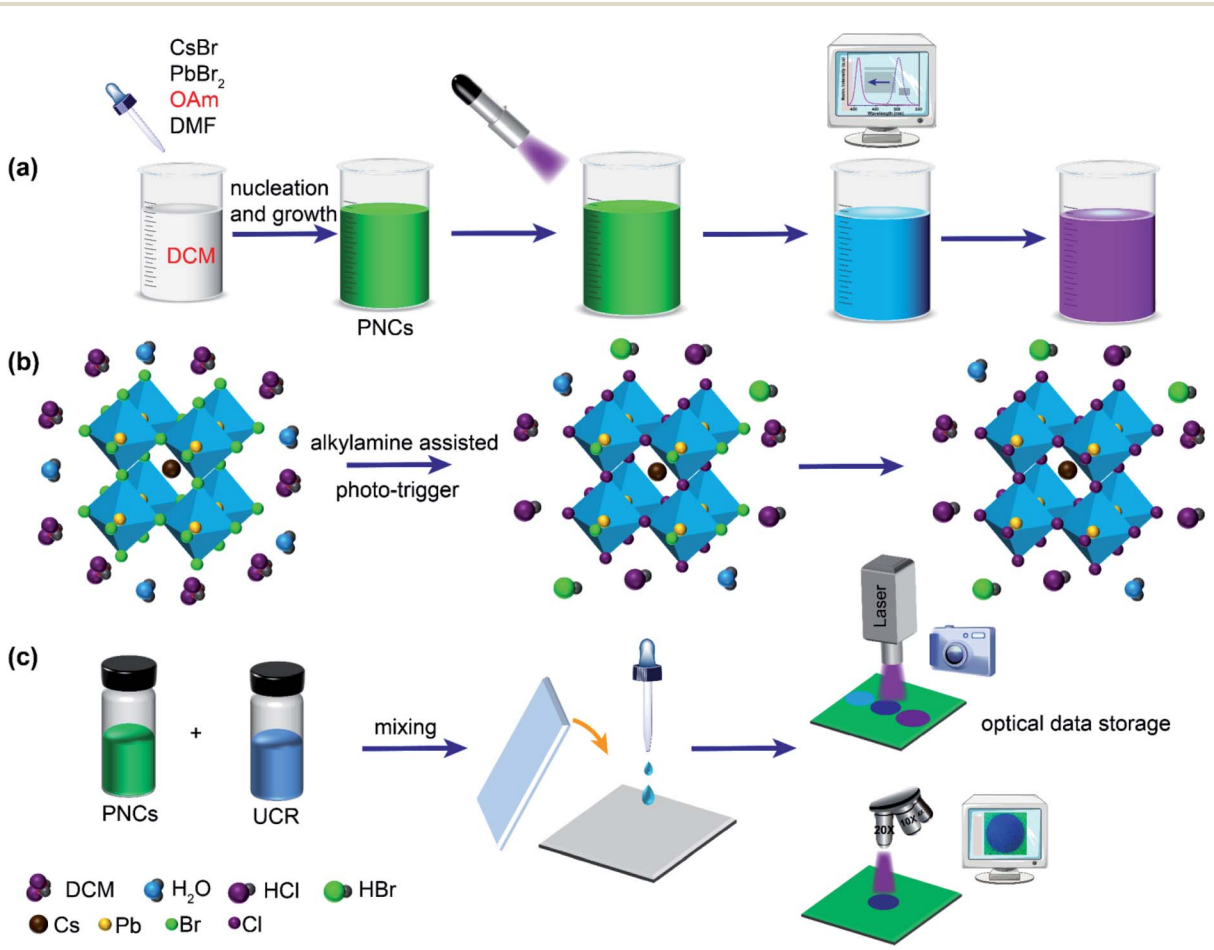

Scheme 1 (a) Schematic illustration of the synthesis and UV-triggered color modulation of the OAm-$CsPbBr_3$ PNCs-DCM system. (b) Schematic illustration of anion-exchange within the cubic perovskite nanocrystal structure from $CsPbBr_3$ to $CsPb(Cl_xBr_{(1-x)})_3$ with the aid of alkylamine ligands and photostimulus. (c) Schematic illustration of the fabrication of the PNCs-UCR-DCM film for optical data storage and writing data with UV light.

Results and discussion

Sunlight and UV light induced fluorescence color change of OAm-$CsPbBr_3$ PNCs in DCM

In order to confirm our accidental discovery of the sunlight-induced fluorescence color change (from green to blue) of OAm-$CsPbBr_3$ PNCs in DCM, we put a bottle of OAm-$CsPbBr_3$ PNCs in DCM outdoor under the sun together with a bottle of OAm-$CsPbBr_3$ PNCs in toluene, and investigated the fluorescence color change of these two solutions from time to time during their exposure to the sunlight (video S1†). It can be clearly observed that PNCs in DCM changed their fluorescence color significantly from green to blue (right bottles in Fig. S1A–D†). By contrast, PNCs in toluene did not change their fluorescence color (green) at all during exposure to sunlight (left bottles in Fig. S1A–D†). This experiment shows the reproducibility of the sunlight-induced fluorescence color change of PNCs in DCM.

It is well known that sunlight contains a large amount of UV light, which can degrade or even destroy organic compounds. Therefore, it was assumed that the solar UV light played a key role in the fluorescence color change of PNCs in DCM. The hypothesis was verified by the fact that PNCs in DCM rather than in toluene displayed a change in their fluorescence (also from green to blue) upon exposure to 365 nm UV light for a while (see Fig. S1E–F, and video S2†). Meanwhile, it is confirmed that DCM is also essential for the light-induced fluorescence color change. For further investigating the effect of UV light illumination on the fluorescence color change of the OAm-PNCs-DCM system, both fluorescence images and emission spectra were recorded for the OAm-PNCs-DCM system after different UV-exposure times (*e.g.* 1 min interval). Fig. 1A shows that the fluorescence color of OAm-PNCs-DCM changed step by step from an initial pure green, to cyan, to blue, and to a final violet during the 1 to 20 min UV-exposure. It should be noted here that the fluorescence photos shown in Fig. 1A were captured for the OAm-PNCs-DCM dispersions contained in homemade circular glass cells (Fig. S2†). In the meantime, the normalized FL spectra clearly show that the maximum emission wavelength of OAm-PNCs-DCM blue-shifted gradually from 512 nm to 417 nm (Fig. 1B). Longer the UV-exposure time, shorter the fluorescence wavelength. This indicates that the fluorescence wavelength of OAm-PNCs-DCM can be easily and precisely tuned by the UV-light (Fig. S3†). Subsequently, UV light induced fluorescence change was investigated for OAm-PNCs-DCM over a wider exposure time range, *e.g.* from 0 to 30 min. It is evident that both fluorescence wavelength and intensity are dependent on the UV exposure time (Fig. 1C). Overall, the fluorescence wavelength red-shifts with increasing exposure time, showing a quasi "S-shape" kinetic response curve (cyan curve in Fig. S4A†). In the ranges of 0–7, 8–19, and 20–25 min, the blue-shift rates are found to be 2.64, 6.22, and 2.54 nm min^{-1}. After 25 min (*i.e.* 26–30 min), almost no blue-shift can be observed, *i.e.* the wavelength of OAm-PNCs-DCM remains constant at 412 nm. The kinetics of UV-induced color change is determined by both the photo-generated rate of Cl^- ions from DCM and the ion exchange between Cl^- and $CsPbBr_3$ PNCs, which will be discussed later in the reaction mechanism investigation. In terms of fluorescence intensity, it increases with UV exposure time rapidly in the first domain (0 to 7 min) and then decreases slowly in the following domain (8 to 20 min), and finally maintains a constant value after 20 min (21 to 30 min). The maximum fluorescence intensity locates at 7 min (pink curve in Fig. S4A†), or at 499.5 nm (pink curve in Fig. S4B†). The relative maximum fluorescence intensity of OAm-PNCs-DCM during UV-exposure varies from an initial 100% (at 518 nm) to 507% (at 499.5 nm), and finally to 26% (at 412 nm), showing a characteristic wavelength-dependent,[58] and UV-enhanced[59] fluorescence quantum yield of PNCs.

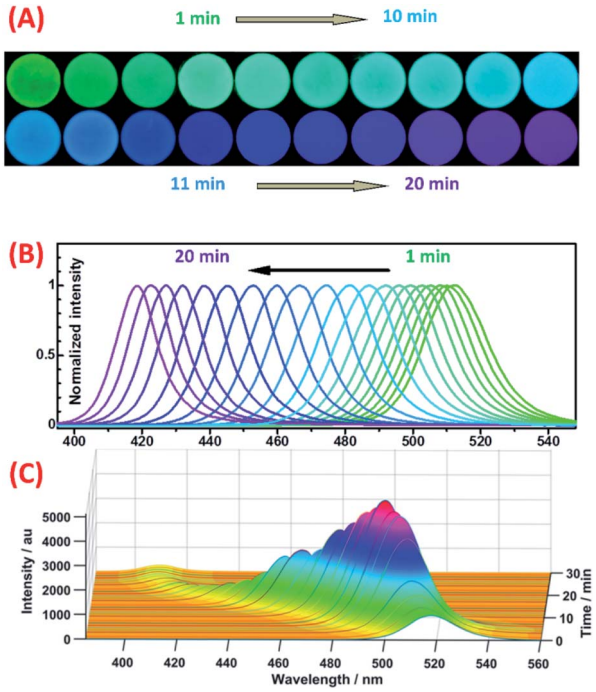

Fig. 1 Fluorescence color variation of OAm-$CsPbBr_3$ PNCs-DCM upon exposure to UV radiation: (A) fluorescence photos and (B) normalized emission spectra obtained for OAm-$CsPbBr_3$ PNCs-DCM at different UV radiation times (1 to 20 min); (C) intensity and wavelength change of OAm-$CsPbBr_3$ PNCs-DCM fluorescence with UV radiation time (0 to 30 min).

After realizing the fact that UV light could continuously tune the fluorescence wavelength of OAm-PNCs-DCM, we were interested to know whether the other light source (*e.g.* white light) could yield the same result. Unfortunately, the wavelength of OAm-PNCs-DCM with illumination of white light did not exhibit an obvious shift during the 30 min exposure (green line in Fig. S5†), while OAm-PNCs-DCM with UV light treatment showed remarkable blue shifts (pink line in Fig. S5†).

Characterization of the structure and composition of PNCs during UV light-induced fluorescence color change

It has been recognized that the emission wavelength of $CsPbX_3$ PNCs is dependent on the composition, *i.e.* the type and ratio of halogen (X = Cl^-, Br^- and I^-) in the nanocrystal,[48] or the

nanoparticle size.[47,60] In order to reveal the origin of the fluorescence color change during the UV exposure process, the variations in optical properties, crystal structure and composition of PNCs were investigated in detail. In a designed experiment, OAm-$CsPbBr_3$ PNCs-DCM solutions were exposed to UV light for 0, 9, 12, 16, 21 min, and the fluorescence emission spectra, UV-vis absorption spectra, and XRD patterns of the resultant OAm-PNCs were parallelly recorded and are shown in Fig. 2. The OAm-PNC solutions have maximum emission peaks respectively at 518, 492, 475, 445 and 417 nm after above 0–21 min UV exposure (Fig. 2A). Meanwhile, the UV-vis absorption band shows similar blue-shifts (Fig. 2B). The Tauc plots (Fig. S6†) educed from the UV-vis data show that OAm-PNCs have increasing bandgap energies (E_g: 2.36, 2.49, 2.59, 2.71 and 2.93 eV) with increasing UV-treatment time. The strong scattering signals of XRD patterns reveal that all these samples have high crystallinity, and the cubic perovskite phases can be preserved throughout the whole irradiation process (Fig. 2C). However, all XRD peaks shift to larger values after the UV irradiation, and longer the UV irradiation time larger the 2θ value. For example, (200) peaks show increasing values, *i.e.* 30.42°, 30.70°, 30.92°, 31.26°, and 31.76° during the continuous irradiation process, which implies that the lattice shrinkage of PNCs might be induced by the doping of Cl^- ions.

Fig. 3A provides the TEM images of OAm-PNCs extracted from OAm-$CsPbBr_3$ PNCs-DCM solutions after 0, 15, and 30 min UV-irradiation. The low resolution TEM images (a–c in Fig. 3A) show that OAm-PNCs retain their cubic shapes after the UV-exposure. The size of OAm-PNCs shows a slight decrease (from 15.8 to 12.7 nm) after the 30 min UV-irradiation of OAm-$CsPbBr_3$ PNCs-DCM solutions (Fig. S7†). However, the slight change in particle size does not correspond to the obvious fluorescence color change (from green to violet), since it has been reported that OAm-$CsPbBr_3$ PNCs with sizes ranging from 20.9 to 13.1 nm basically emit green light (514 nm).[61] The high resolution TEM images (d–f in Fig. 3A) indicate that the extracted OAm-PNCs after 0, 15, and 30 min UV irradiation respectively have lattice spacing values of 0.587, 0.572 and 0.564 nm. The decrease in lattice spacing implies that other halogen ions, most likely smaller Cl^- ions are doped into OAm-$CsPbBr_3$ PNCs. The doping of Cl^- into OAm-$CsPbBr_3$ PNCs is further verified by EDX spectroscopy (Fig. S8†) and EDX elemental mapping (Fig. 3B) obtained for the purified PNCs from the OAm-$CsPbBr_3$ PNCs-DCM system irradiated by UV for 15 min.

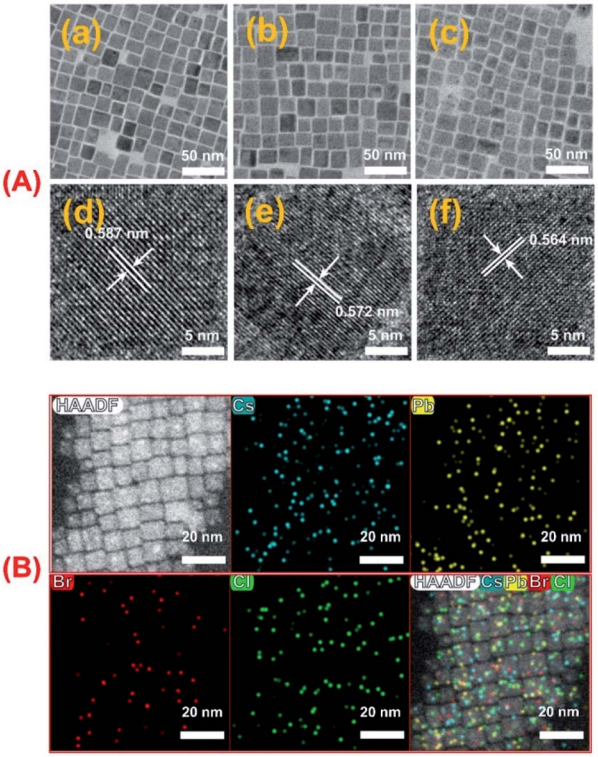

Fig. 3 (A) TEM images obtained for OAm-PNCs after exposing OAm-$CsPbBr_3$ PNCs-DCM to UV for 0 min (a and d); 15 min (b and e) and 30 min (c and f). (B) EDX elemental mapping images obtained for OAm-PNCs after exposing OAm-$CsPbBr_3$-DCM to UV for 15 min. All OAm-PNC samples for TEM and EDX mapping measurements were centrifuged from OAm-$CsPbBr_3$-DCM solutions and washed with toluene 3 times.

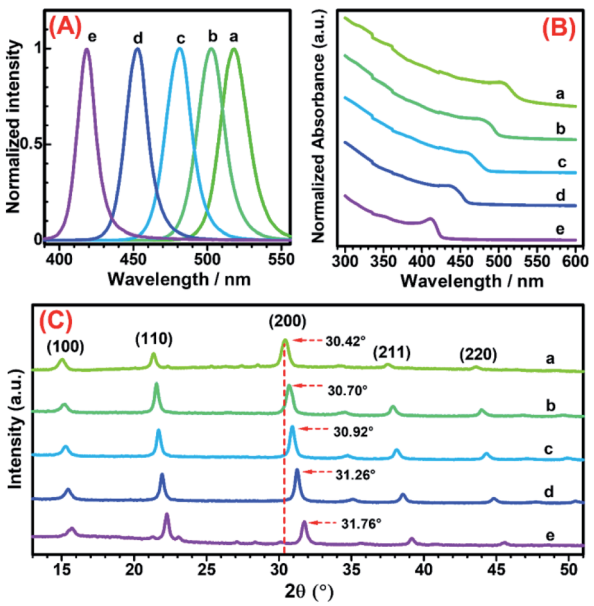

Fig. 2 (A) Fluorescence emission spectra, (B) UV-vis absorption spectra, and (C) powder X-ray diffraction (XRD) patterns parallelly measured for OAm-$CsPbBr_3$-DCM after UV-exposure for different times: (a) 0; (b) 9; (c) 12; (d) 16; (e) 21 min.

It can be concluded from the above spectrum and morphology investigations that the fluorescence color change of the OAm-$CsPbBr_3$ PNCs-DCM system during UV irradiation essentially results from the doping of the photo-generated Cl^- ion into OAm-$CsPbBr_3$ PNCs.

Mechanism of the photo-induced fluorescence color change based on the OAm-$CsPbBr_3$ PNCs-DCM system

As mentioned above, upon UV-exposure, OAm-$CsPbBr_3$ PNCs can change their fluorescence color in DCM rather than in

toluene, which suggests that DCM may play an important role in the photo-triggered color change. To clarify the effect of the dispersion solvent, the investigated dispersion solvents were extended from the two types of solvents to six types of non-polar solvents, including DCM, benzene, toluene, *n*-hexane, cyclohexane and ethyl ether. Before UV-irradiation, PNCs in all solvents emit green light (Fig. S9A†). After 10 min UV-treatment, only PNCs in DCM emit blue light whereas PNCs in all other solvents maintain their green fluorescence (Fig. S9B†). This more detailed investigation on the effect of dispersion solvent further verifies that DCM is essential in the photo-triggered color change. In terms of molecular structure, each DCM molecule contains two chlorine (Cl) atoms, which means that the Cl atoms in DCM molecule cannot undergo ion exchange with the PNCs directly. This can be proved by the fact that OAm-$CsPbBr_3$ PNCs in DCM retain the green fluorescence for a long time in the absence of UV irradiation. However, it is evident from XRD and TEM data that ion exchanges between OAm-$CsPbBr_3$ PNCs and Cl^- ions are indeed involved in the color change. Therefore, it can be assumed that the Cl^- ions for the ion exchanges are provided by UV-induced degradation of DCM. The assumption is reasonable since UV-degradation of DCM into HCl (eqn (1) and (2)) in the presence of catalysts has been reported in several literature studies:[62–64]

$$CH_2Cl_2 \xrightarrow{h\nu} Cl\bullet + \bullet CH_2Cl \quad (1)$$

$$Cl^{\bullet} + CH_2Cl_2 \Leftrightarrow HCl + {}^{\bullet}CHCl_2 \quad (2)$$

Subsequently, the degradation of DCM in the OAm-PNCs-DCM system by UV radiation was monitored by measuring the variation of the characteristic Raman peak, 703 cm^{-1} of DCM (Fig. 4A). It is evident that DCM degrades with UV-exposure time over 0 to 30 min, and shows an "S" shape curve (Fig. 4B), which is quite similar to the plot of wavelength *vs.* UV irradiation time (Fig. S4A†). The similarity in kinetic response (*i.e.* S-shape) implies that the UV-induced fluorescence color change might be determined by the degradation of DCM. After 30 min UV irradiation, 46.8% of DCM can be found to be degraded. In contrast, pure DCM (in the absence of OAm-PNCs) is hardly degraded over 30 min UV-treatment (Fig. 4C). The obvious difference in degradation rate suggests that OAm-PNCs like TiO_2[63] may act as an efficient catalyst for DCM UV-degradation.

In addition to the dispersion solvent (DCM), the alkylamine capping ligands on PNCs were also found to play another key role in the photo-induced fluorescence color change. So far, OAm capped PNCs (*i.e.* OAm-PNCs) are being investigated for their fluorescence color change in DCM upon UV irradiation. Actually, OA and OAm bi-ligand capped PNCs (*i.e.* OA/OAm-PNCs), the most common PNCs, were first found to have photo-responsive luminescence activity in DCM (Fig. S10a†). In order to investigate the effect of the ligand separately, we synthesized two kinds of sole-ligand capped PNCs, *i.e.* OA-PNCs and OAm-PNCs. As mentioned above, OAm-PNCs can change fluorescence color in DCM by exposure to UV radiation (also refer to Fig. S10b†). In contrast, OA-PNCs do not change their emission wavelength in DCM upon UV exposure at all

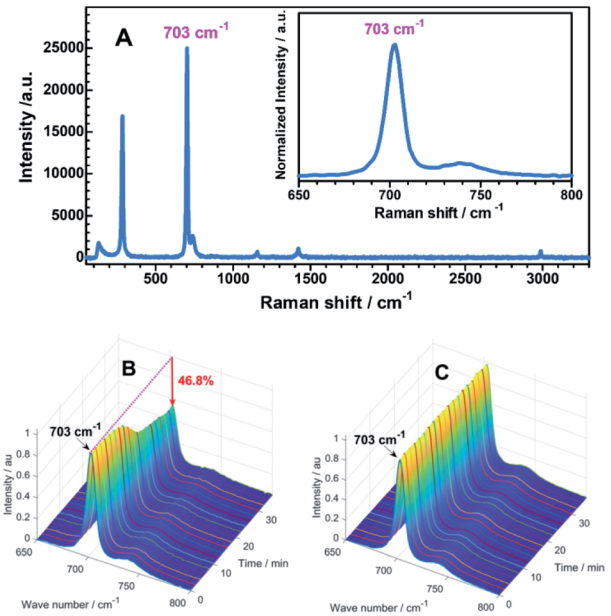

Fig. 4 Typical Raman spectrum of pure DCM (A); variation of the Raman peak (703 cm^{-1}) of DCM with UV-exposure time in the presence (B) and absence (C) of OAm-PNCs.

(Fig. S10c†). This difference in optical property suggests that OAm or some other alkylamine capping is important for the emission wavelength change. To verify this hypothesis, another alkylamine, for example octadecylamine (ODA) was used as the sole capping ligand to synthesize ODA-PNCs dispersed in DCM. As expected, a significant blue shift of emission can be observed for the ODA-PNCs-DCM system upon UV exposure (Fig. S11 and S12a†). Meanwhile, another alkylacid, *e.g.*, stearic acid (SA) capped PNCs in DCM was investigated, but there was no observable shift in the maximum emission wavelength of SA-PNCs (Fig. S12b†). Therefore, it is verified that alkylamine ligands rather than alkylacid ligands play another crucial role in the photo-induced fluorescence color change.

It is well known that alkylamines ($R–NH_2$) are proton acceptors, thus they can react with photo-generated HCl molecules from DCM to form protonized alkylamine ($R–NH_3^+$) ions and release free Cl^- ions (eqn (3)), followed by ion exchange with $CrPbBr_3$ PNCs (eqn (4)) and recovery of $R–NH_2$ (eqn (5)). Apparently, the alkylamine molecules capping on the surfaces of PNCs may accelerate the photo-induced ion exchange. Herein, it should be pointed out that the ion exchange-acceleration effect of the alkylamine capping ligands is based on the photocatalytic degradation of DCM by PNCs (eqn (1) and (2)), since no obvious DCM degradation can be observed by Raman spectroscopy in the presence of only an alkylamine (*e.g.* OAm) rather than alkyamine + PNCs (*e.g.* OAm-PNCs) as shown in Fig. S13.†

$$R–NH_2 + HCl \Leftrightarrow R–NH_3^+ + Cl^- \quad (3)$$

$$xCl^- + CsPbBr_3 \Leftrightarrow CsPbBr_{3-x}Cl_x + xBr^- \quad (4)$$

$$R\text{–}NH_3^+ + Br^- \Leftrightarrow R\text{–}NH_2 + HBr \quad (5)$$

Both OAm capped PNCs and OA/OAm capped PNCs undergo a change in their emission wavelength in DCM under UV irradiation as they both bear alkylamine molecules at their surfaces, however, the UV-stability of OAm-PNCs is much better than that of OA/OAm-PNCs (Fig. S14†). Moreover, the preparation of sole-ligand capped PNCs is simpler and less expensive than that of bi-ligand capped PNCs. Therefore, OAm-PNCs-DCM rather than OA/OAm-PNCs-DCM was selected as the PLM.

As demonstrated above, UV irradiation is essential for fluorescence color change, then the UV irradiation power may affect the variation rate of emission wavelength. In our investigation, UV beams with relative irradiation powers of 100%, 25%, 12.5% and 3.125% were supplied by passing the same UV light beam through different power-cutting filters (1, 1/4, 1/8, and 1/32), and applied to the OAm-PNCs-DCM system. It can be found that a higher UV irradiation power can result in a faster wavelength change (Fig. S15†), which implies that a very fast fluorescence color change (*e.g.* in ms scale) can be achieved if a high power UV beam (*e.g.* a UV laser beam) is adopted.

UV light induced fluorescence color change with a super wide color gamut based on the OAm-CsPb($Br_{0.4}I_{0.6}$)$_3$ PNCs-DCM system

After realizing the photo-induced fluorescence color change from green to violet based on the green-emissive OAm-$CsPbBr_3$ PNCs-DCM system, we tried to apply the same strategy to the red-emissive OAm-CsPb($Br_{0.4}I_{0.6}$)$_3$ PNCs-DCM system for obtaining a photo-induced color change over a wider color gamut. Our investigation shows that the fluorescence color of the OAm-CsPb($Br_{0.4}I_{0.6}$)$_3$ PNCs-DCM system can be tuned with the help of UV light irradiation from an initial red to orange, yellow, green, cyan, blue and finally violet in that order (Fig. 5A). Correspondingly, the maximum emission wavelength shifts from 635 nm to 409 nm with increasing irradiation time (Fig. 5B), showing a super wide color gamut (Fig. S16†). Similar to the green PNCs-DCM system, the red PNCs-DCM system also shows variable emission intensity during the UV-light irradiation (Fig. 5C). However, unlike the green PNCs-DCM system that has the maximum emission at 499.5 nm (Fig. 1C), the red PNCs-DCM system has the maximum emission at the beginning (*i.e.* without light irradiation), then decreases its fluorescence quantum yield during color change from red to green with the minimum value around 500 nm, finally the fluorescence quantum yield recovers to a certain value around blue and violet color zones (Fig. 5C). Probably, the difference in the variation of emission quantum yield between the red PNCs-DCM and green PNCs-DCM systems might result from different mechanisms involved in the light-induced color change.

Firstly, red PNCs that contain easily reduced I^- are sensitive to light, especially UV light irradiation. It was observed that the red PNCs (CsPb($Br_{0.4}I_{0.6}$)$_3$) could blue-shift their fluorescence even in toluene, *i.e.* in the absence of DCM (orange dots in Fig. S17†), which means that UV-light irradiation alone can induce fluorescence color change without halogen ion

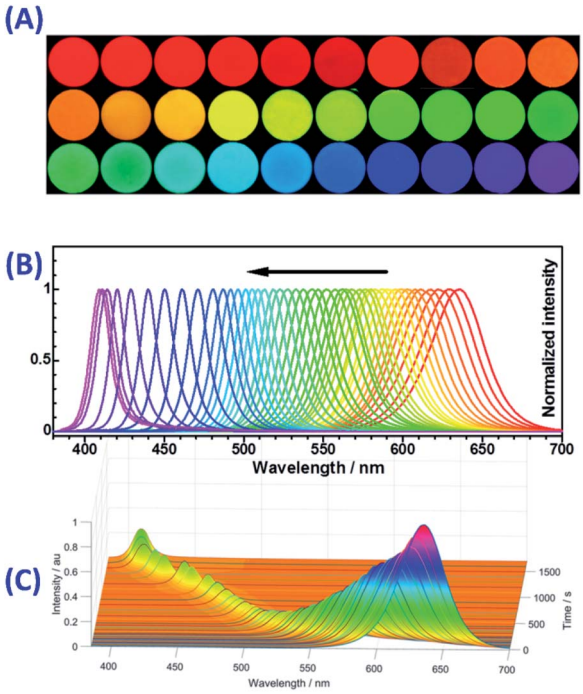

Fig. 5 Fluorescence color variation of OAm-CsPb($Br_{0.4}I_{0.6}$)$_3$ PNCs-DCM upon exposure to UV radiation: (A) fluorescence photos and (B) normalized emission spectra obtained for OAm-CsPb($Br_{0.4}I_{0.6}$)$_3$ PNCs-DCM at different UV radiation times (0 to 1500 s); (C) intensity and wavelength change of OAm-CsPb($Br_{0.4}I_{0.6}$)$_3$ PNCs-DCM fluorescence with UV radiation time (0 to 1500 s).

exchange. The blue-shift in the fluorescence wavelength of the red PNCs may result from that light irradiation decomposes I^- ions in the CsPb($Br_{0.4}I_{0.6}$)$_3$ crystals into I_2 and PbO.[65,66] The photo-oxidation of I^- and subsequent release of photo-generated I_2 into the solution phase causes a decrease in the ion number ratio of I^- to Br^- in the PNCs (R_{I^-/Br^-}) from the initial value of 1.5 (*i.e.* red emissive CsPb($Br_{0.4}I_{0.6}$)$_3$ PNCs with λ_{max} = 635 nm) to a lower value (*e.g.* R_{I^-/Br^-} = 1.0 for CsPb($Br_{0.5}I_{0.5}$)$_3$ with λ_{max} = 600 nm).[67] The photolysis of CsPb($Br_{0.4}I_{0.6}$)$_3$ PNCs is proposed in eqn (6) and S1–S5,† in which it was assumed that the ratios of R_{I^-/Br^-} in the crystal and solution were the same. If 1.5 O_2 molecules take part in the photolysis reaction, then we can obtain eqn (7). In this case, CsPb($Br_{0.5}I_{0.5}$)$_3$ PNCs with orange fluorescence can be obtained. However, the fluorescence color change is obviously slowed down after 550 nm, probably due to the depletion of dissolved O_2 in toluene and residue of some I^- ions in the nanocrystals. In that case, it is very difficult for CsPb(Br_xI_{1-x})$_3$ PNCs to change their fluorescence color to green without their ion exchange with Br^- or Cl^-.

Apparently, the photo-induced oxidation of I^- ions by O_2 can also be observed in DCM (pink dots in Fig. S17†); moreover, the photo-generated HCl from DCM would enhance the oxidation ability of O_2 by providing protons (H^+). Therefore, both the photo-induced oxidation of I^- into I_2 by O_2, and the ion exchanges among Br^-, I^- and photo-generated Cl^- (eqn (8)) would shift the fluorescence color from red to green or even to violet (Fig. 5). For example, if 3 molecules of dissolved O_2 and 12

molecules of photo-generated HCl are involved in the oxidation and ion exchange reactions with 10 particles of $CsPb(Br_{0.4}I_{0.6})_3$ PNCs, then 10 $CsPb(Cl_{0.4}Br_{0.4}I_{0.2})_3$ PNCs can be obtained (eqn (9)). To further verify the reaction mechanism shown in eqn (8), a series of $CsPb(Cl_xBr_{0.4}I_{(0.6-x)})_3$ and $CsPb(Cl_{x/(1+x)}Br_{0.4/(1+x)}I_{0.6/(1+x)})_3$ PNCs were prepared and investigated. $CsPb(Cl_xBr_{0.4}I_{(0.6-x)})_3$ PNCs were synthesized by keeping the amount of Br^- unchanged while decreasing the amount of I^- and simultaneously increasing the amount of Cl^- to simulate the photo-induced oxidation coupled with ion exchange processes (eqn (8)). $CsPb(Cl_{x/(1+x)}Br_{0.4/(1+x)}I_{0.6/(1+x)})_3$ PNCs were prepared by keeping the amount of Br^- and I^- unchanged while increasing the amount of Cl^- to simulate sole photo-induced ion exchange processes (eqn (S6)†). By comparison, it is evident that the fluorescence spectra and their variation trends measured for the UV-irradiated $CsPb(Br_{0.4}I_{0.6})_3$ PNCs-DCM system (Fig. 5) are very similar to those investigated for the $CsPb(Cl_xBr_{0.4}I_{(0.6-x)})_3$ stimulation system over the whole wavelength ranges (Fig. S18 and Table S2†), but obviously different from those recorded for the $CsPb(Cl_{x/(1+x)}Br_{0.4/(1+x)}I_{0.6/(1+x)})_3$ PNC stimulation system (Fig. S19 and Table S3†). In detail, both the UV-irradiated $CsPb(Br_{0.4}I_{0.6})_3$ PNCs-DCM system and $CsPb(Cl_xBr_{0.4}I_{(0.6-x)})_3$-PNCs-DCM stimulation system have relatively high fluorescence intensity over the wavelength ranges of 635–555 nm and 477–421 nm (Fig. 5C and Table S2†), and both have the lowest intensity around 500 nm. In contrast, the sole ion exchange system, *i.e.*, $CsPb(Cl_{x/(1+x)}Br_{0.4/(1+x)}I_{0.6/(1+x)})_3$ PNC stimulation system has a relatively high fluorescence quantum yield in a narrow wavelength range of 635–585 nm, and very low fluorescence activity in most regions of the wavelength range (Table S3†). The low fluorescence quantum yields around 500 nm (523–479 nm) for the $CsPb(Cl_xBr_{0.4}I_{(0.6-x)})_3$ PNC stimulation system may be because there are comparable amounts of Cl^-, Br^- and I^- ions in the system (*i.e.*, $Cl^- : Br^- : I^- \approx 1 : 1 : 1$), for example, 2.25 : 4 : 3.75; 2.5 : 4 : 3.5; 3 : 4 : 3; or 3.5 : 4 : 2.5 (Table S3†). It has been reported that $CsPb(Cl : Br : I)_3$ PNCs have a very low fluorescence quantum yield (<0.1%).[68] In brief, the above experimental data suggest that eqn (8) can be used to well explain the photo-induced fluorescence color change mechanism for the $CsPb(Br_{0.4}I_{0.6})_3$ PNCs-DCM system.

$$10CsPb(Br_{0.4}I_{0.6})_3 + xO_2 \xrightarrow{hv} (10-2x)CsPb\left(Br_{\left(0.4+\frac{16x}{300-40x}\right)}I_{\left(0.6-\frac{16x}{300-40x}\right)}\right)_3 + 2xPbO + 2xI_2 + 2xCs^+ + 2x\left(0.4+\frac{16x}{300-40x}\right)Br^- + 2x\left(0.6-\frac{16x}{300-40x}\right)I^- \quad (6)$$

$$10CsPb(Br_{0.4}I_{0.6})_3 + 1.5O_2 \xrightarrow{hv} 7CsPb(Br_{0.5}I_{0.5})_3 + 3PbO + 3I_2 + 3Cs^+ + 1.5Br^- + 1.5I^- \quad (7)$$

$$10CsPb(Br_{0.4}I_{0.6})_3 + 3xO_2 + 12xHCl \rightarrow 10CsPb(Cl_{0.4x}Br_{0.4}I_{(0.6-0.4x)})_3 + 6xI_2 + 6xH_2O \quad (8)$$

$$10CsPb(Br_{0.4}I_{0.6})_3 + 3O_2 + 12HCl \rightarrow 10CsPb(Cl_{0.4}Br_{0.4}I_{0.2})_3 + 6I_2 + 6H_2O \quad (9)$$

Optical data recording strategy based on the OAm-$CsPbX_3$ PNCs-DCM system

The facile synthesis, high color purity, wide color gamut and excellent phototriggered fluorescence tunability of the PNCs-DCM system inspired us to develop a new optical data recording medium. It turned out that the optical recording medium can be fabricated in a simple way. Briefly, the PNCs-DCM solution is blended with some UV cure resin (UCR) and dropped on a clean glass substrate, and PNCs-UCR-DCM film (*ca.* 160 μm thick) is formed after placing a thin cover slip on the top (Fig. 6A). The addition of UCR not only significantly improves the viscosity of the film to avoid diffusion of PNCs therein, but also easily solidifies the film after UV irradiation to well maintain photo-painting patterns. The obtained PNCs-UCR-DCM film is transparent (Fig. S20A†) under white light and emits uniform and green light under a 365 nm UV light (Fig. S20B†). Before using the PNCs-UCR-DCM film for optical data recording, the effect of UCR on the optical properties of PNCs-DCM was evaluated first. The fluorescence intensity of UCR is weak enough to be omitted both before and after UV irradiation (Fig. S21A†), which means that the very weak UCR emission does not affect the strong fluorescence of PNCs-DCM during the UV radiation process. Additionally, the introduction of UCR into the PNCs-DCM system only causes a slight decrease in fluorescence intensity, and a small redshift of the emission peak (Fig. S21B†), which might result from the slight aggregation of hydrophobic PNCs in the presence of the weakly polar UCR. Overall, the use of UCR in the film does not obviously change the optical performances of the PNCs-DCM system. Therefore, the prepared PNCs-UCR-DCM film can be further investigated for optical data recording as follows.

First, a UV-light beam from an inverted microscope (×20) was used to draw patterns on the PNCs-UCR-DCM film to validate the UV light beam as a photo-painter (Fig. 6A). A clear blue emissive disk-shaped pattern can be observed on the green emissive film during a short period (0–15 s) of UV-light irradiation (Fig. 6B), showing that the PNCs-UCR-DCM film is a fast-responsive photochromic medium. After UV-light irradiation for 15 s, the disk-shaped pattern has a strong signal at the blue channel while it shows weak intensity at the green channel (Fig. 6C), suggesting that the fluorescence is changed from green to blue after the UV irradiation. Additionally, more complicated (*e.g.* disk-ring shaped) patterns can also be obtained by appropriate UV-light exposure (Fig. 6D).

Subsequently, a computer-controlled 355 nm UV laser beam was applied to produce patterns on the PNCs-UCR-DCM film (Fig. 7A). Similar to the UV light beam from a microscope mentioned above, the computer-controlled UV laser beam can

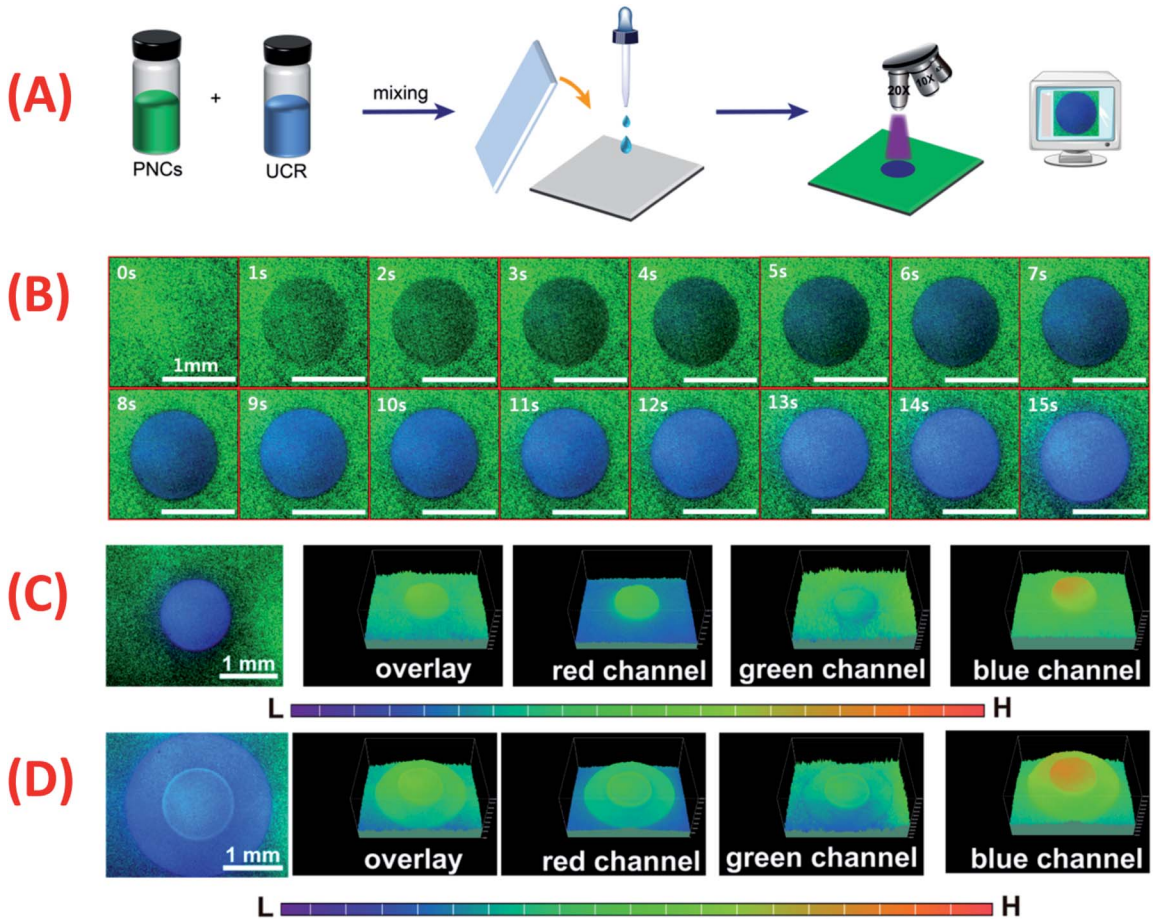

Fig. 6 (A) Schematic diagram for the fabrication of PNCs-UCR-DCM film and optical writing with UV-light. (B) Blue emissive disk-shaped patterns optically written on the green emissive PNCs-UCR-DCM film at different UV-irradiation times (0 to 15 s). (C) The fluorescence image of a disk-shaped pattern and its RGB channel images. (D) The fluorescence image of the disk/ring-shaped pattern and its RGB channel images.

also mark a clear blue-emissive pattern on the green-emissive PNCs-UCR-DCM substrate (section (a) in Fig. 7B). Moreover, the laser produced pattern has even more uniform color distribution and clearer edge due to the fact that a scanning laser beam can provide more uniform UV irradiation on a substrate than a UV beam from the microscope. Fluorescence emission wavelength was measured for the printed disk pattern and its adjacent intact NCs-UCR-DCM film along the *X*-axis (orange dashed lines in Fig. 7B-(a) and B-(b)) and *Y*-axis (pink dashed lines in Fig. 7B-(a) and B-(c)). For the selected pattern (*i.e.* for 50-time laser scanning) shown in Fig. 7B-(a), the sampling points of the intact film all have fluorescence wavelength around 516 nm while the sampling points within the light-printed disk area all have an emission wavelength of 470 nm, showing the very sharp edge and the good consistency in wavelength. For a relatively shorter laser irradiation (*e.g.* 20-time laser scanning), similar good results can be obtained, except that the printed disk pattern gives 495 nm fluorescence (Fig. S22†). The clear edge and uniform wavelength distribution of the laser-marked patterns on the PNCs-UCR-DCM film enable data to be accurately written and read by laser. Additionally, the bright, uniform and clear-edged fluorescence patterns on the film can be maintained over the investigated 15 days without any visible destruction (Fig. S23A†), showing their good storage stability. This merit may be attributed to the unique fluorescence color change mechanism based on the UV-induced ion exchange. As demonstrated above, UV irradiation, alkylamine-capped PNCs, DCM and ion exchange are all essential for the fluorescence color change. Without any of these conditions at the beginning, *e.g.* UV exposure (Fig. S5†), or OAm-PNCs (Fig. S10†), or DCM (Fig. S1 and S9†), or ion exchange (Fig. 3), the fluorescence color change of PNCs does not happen. Similarly, the removal of any of these conditions during the reactions, *e.g.* stopping the UV irradiation (Fig. S23B and C†), or removing DCM (the source of halogen ions) after optical writing, or solidifying the film (preventing ion exchange) will lead to the immediate ceasing of color change, without any delay. By controlling laser scanning cycles, laser-marked patterns with different fluorescence colors can be obtained (Fig. 7C), which means information related to laser scanning cycles can be written on the PNCs-UCR-DCM film. Moreover, the parallelly ($n = 7$) fabricated patterns by the computer-controlled laser beam at different irradiation times (or scanning cycles) have shown very good reproducibility (Fig. 7D), implying that sufficiently stable optical data writing can be archived. Finally, time (or scanning cycle)-dependent optical writing was

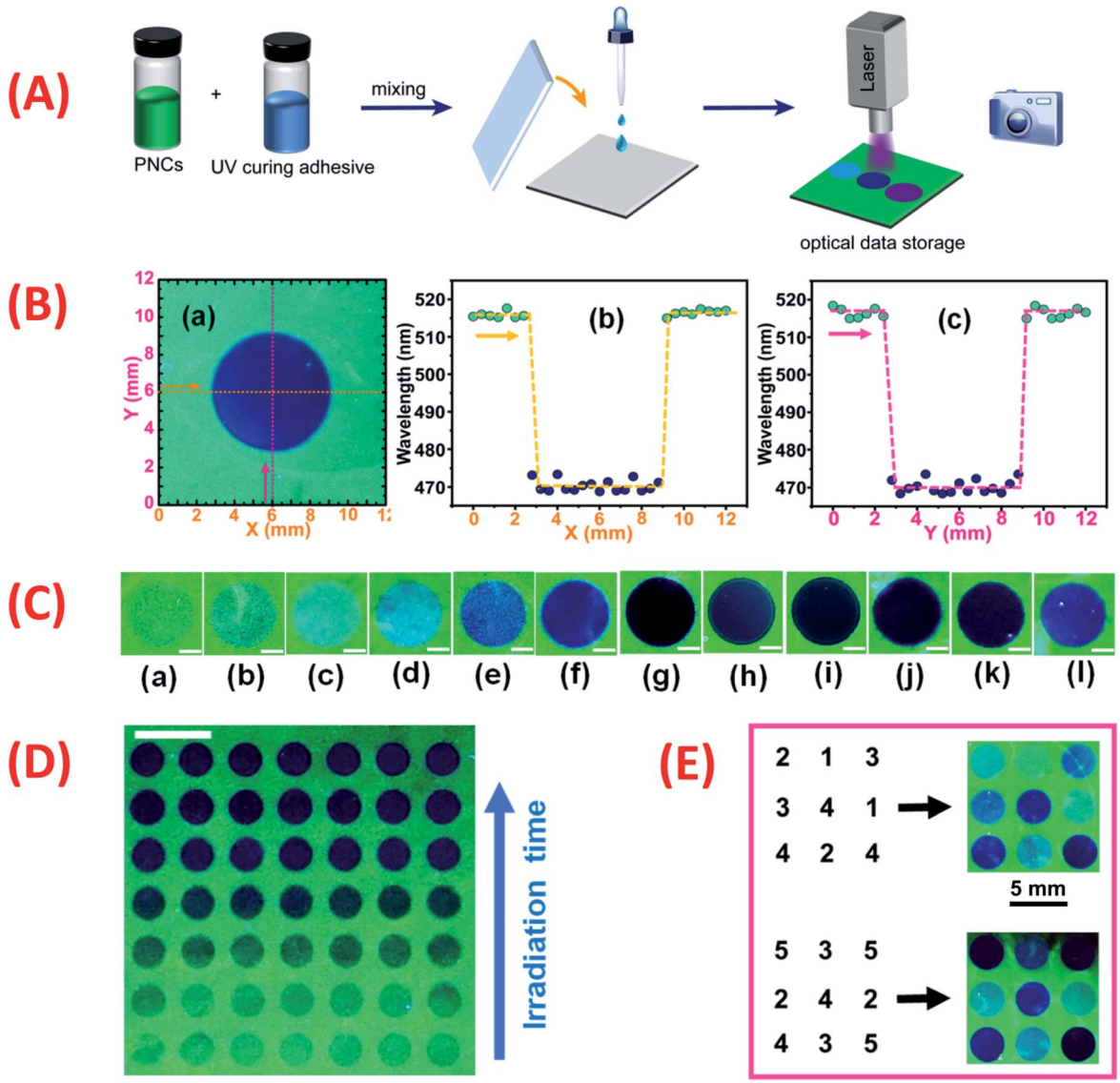

Fig. 7 (A) The overall procedures of fabrication of PNC-based optical data storage using a UV-laser beam as a recording pen. (B) Blue emissive disk-shaped pattern (a) painted on a green emissive PNC thin film by a 355 nm laser beam (50 scans), and the maximum emission wavelengths probed along the *X*-axis (b) and *Y*-axis (c) using a USB fiber optical spectrophotometer. (C) Blue emissive disk-shaped patterns obtained on the PNC film at different UV-laser scans: (a) 5; (b) 10; (c) 15; (d) 20; (e) 30; (f) 40; (g) 50; (h) 60; (i) 70; (j) 80; (k) 90; (l) 100. (D) Repeated fabrication (n = 7) of laser-painted patterns at different 355 nm-laser irradiation times (or scans). (E) Digital information (related to laser scan number or emission wavelength) written on the PNC film. Scale bars are 2 mm in all images.

performed using the computer-controlled UV laser beam. For example, information of numbers (N) "1", "2", "3", "4", and "5" was written on the PNCs-UCR-DCM film by respectively scanning the UV laser beam on certain points for 10, 20, 30, 40 and 50 cycles, resulting in distinguishable patterns with different fluorescence colors (Fig. 7E). The fact that the fluorescence color of the PNCs-DCM system can be precisely (in several nanometers resolution) tuned over a very wide (~650 to ~410 nm) color gamut (Fig. 5), implies that the N value (number of distinguished fluorescence peaks) would be very large (*e.g.* N = 16 at 15 nm peak wavelength intervals), then each laser-printed spot would have 8 times recording density {coded by (0000), (0001), (0010), (0011), (0100), (0101), (0110), (0111), (1000), (1001), (1010), (1011), (1100), (1101), (1110), and (1111)} as that of single-wavelength PLMs {coded by (0) and (1)}. Therefore, the PNCs-UCR-DCM film may have promising applications in high-density optical data storage. However, further efforts are still required to remove the flaw that the optical data are irreversibly written on the PNC-based film, *i.e.* this new kind of high-density optical data storage device works presently in a read-only mode, for realizing better storage with erasing and re-writing functions in the future.

Conclusions

The wavelength of perovskite nanocrystals (PNCs) in the presence of dichloromethane (DCM) could be continuously and precisely tuned over a very wide color range (from red to violet)

by UV irradiation. The UV-induced fluorescence color change results from the UV light-triggered and PNC-catalyzed dissociation of chlorine anion (Cl^-) from DCM and subsequently alkylamine assisted ion exchange of Cl^- with PNCs. Finally, the PNCs-DCM system with the merits of easy fabrication, wide and precise wavelength tunability, sensitive and fast photoresponse, and only single writing/reading light source requirement has been demonstrated to have promising applications in high-density optical data storage.

Experimental section

Materials and reagents

Lead(II) bromide ($PbBr_2$), cesium bromide (CsBr), *N*,*N*-dimethyl formamide (DMF, 99.5%), oleylamine (OAm, 80–90%), oleic acid (OA, >99.99%), octadecylamine (ODA, 90%) and stearic acid (SA, 95%) were all purchased from Aladdin (China). Dichloromethane (DCM, 99.99%) and toluene (99.7%) were obtained from Sinopharm Chemical Reagent Co., Ltd (China). Loctite 3491UV cure resin was provided by Henkel Co. Ltd, China. All reagents were used as received without further purification.

Measurements and equipment

Transmission electron microscopy (TEM) and high-resolution transmission electron microscopy (HR-TEM), and the scanning transmission electron microscopy energy dispersive X-ray spectroscopy (STEM-EDS) elemental analysis were carried out on a Tecnai G2 F20 S-TWIN microscope (FEI Nano Ports, U.S.A). Photoluminescence (PL) spectra were recorded using an F-4600 fluorescence spectrophotometer (Hitachi, Japan). UV-vis spectra of PNC solutions were recorded using a TU-1950 spectrophotometer (Persee, China). The photos were taken with a Powder-Shot digital camera (Canon, Japan). The X-ray diffraction (XRD) pattern was performed with a D/MAX 2200 VPC powder diffractometer (Rigaku, Japan). A R838 UV lighter (3 W, Warsun, China) was used to provide 365 nm UV irradiation for the PNCs-DCM solutions at a typical distance of 4 cm with an optical power density of 10 mW cm^{-2}. An LS125 UV radiometer (Shenzhen Linshang Technology Co. Ltd, China) was used to measure the radiation intensity of the UV light source. A 355 nm UV laser marking system (5 W, Da Peng Laser) was used to print colorful fluorescence patterns on the PNC films. The spectra of PNC films were recorded with a USB 2000 fluorescence spectrometer (Ocean Optic Inc., USA) combined with a microscope platform. The fluorescence microscopic photos were taken with an Eclipse Ti–U inverted microscope (Nikon, Japan). The quantum yields of PNCs were measured by a previously reported method,[69] as shown in page S31 of the ESI.†

Synthesis of PNCs-DCM solutions

The green-emissive OAm-$CsPbBr_3$ PNCs-DCM solution was prepared as follows: $PbBr_2$ (0.4 mmol), CsBr (0.4 mmol) and OAm (300 μL) were added respectively into DMF (10 mL) and stirred rigorously to form a transparent precursor solution. Then 400 μL of precursor solution was quickly injected into 10 mL of DCM under violent stirring to yield the green emissive OAm-$CsPbBr_3$ PNCs-DCM solution. The concentration of $CsPbBr_3$ PNCs in DCM solution was measured to be 1.9×10^{-3} mol L^{-1} or 1.1 mg mL^{-1} (see the calculation shown in page S30 in the ESI†).

The synthesis of red-emissive OAm-$CsPb(Br_{0.4}I_{0.6})_3$PNCs-DCM was analogous to the method used for OAm-$CsPbBr_3$-DCM, wherein $PbBr_2$ and CsBr were substituted by $PbBr_2$ (0.16 mmol), CsBr (0.16 mmol), PbI_2 (0.24 mmol) and CsI (0.24 mmol).

Preparation of PNCs-UCR-DCM film and optical data writing

Firstly, 250 μL of PNCs-DCM solution with the PNC concentration of 1.1 mg mL^{-1} and 250 μL of UV cure resin were mixed and shaken for 10 min in the dark to yield a uniform and viscous mixture. Then, 70 μL of mixture was carefully dropped on the middle of a glass slide and pressed by a thin coverslip to form a uniform and transparent wet film (2 cm × 2 cm × ~160 μm). The loading of PNCs in the wet film (PNCs-DCM-UCR) was calculated to be 0.047% (page S30 in the ESI†). With an inverted microscope, the fluorescence patterns with various colors were acquired by exposing the PNCs-UCR-DCM film to the UV light beam for different times (0–15 s), while with the 355 nm UV laser marking system, the different fluorescence patterns on the film were printed by scanning the UV laser beam at given sites for different cycles (5 to 100). After printing the fluorescence patterns associated with certain optical data information, the film was put in a well-ventilated place for 15 min to remove residual DCM. In the absence of DCM, the film becomes even more viscous, and the photo-induced ion exchange and fluorescence color changes stop, keeping the fluorescence patterns unchanged. Finally, the PNCs-UCR film printed with fluorescence patterns is solidified with a UV lamp, yielding a dried film thickness of 79.5 ± 9.0 μm ($n = 12$, 95% confidence level). The loading of PNCs in the dried film (PNCs-UCR) was calculated to be 0.11% (page S31 in the ESI†).

Data availability

All data are available in the ESI.†

Author contributions

Yuwu Chi planned and supervised the project, Jie Chen, Zelian Xu, Jingcheng Zheng, Haishan Wu designed and carried out the detailed experiments, Jie Chen analysed the data and wrote the whole paper.

Conflicts of interest

There are no conflicts to declare.

Acknowledgements

This study was financially supported by the National Natural Science Foundation of China (No. 22074018) and the Program

for Changjiang Scholars and Innovative Research Team in University (No. IRT_15R11).

Notes and references

1 O. Sato, *Nat. Chem.*, 2016, **8**, 644.
2 M. A. C. Stuart, W. T. S. Huck, J. Genzer, M. Muller, C. Ober, M. Stamm, G. B. Sukhorukov, I. Szleifer, V. V. Tsukruk, M. Urban, F. Winnik, S. Zauscher, I. Luzinov and S. Minko, *Nat. Mater.*, 2010, **9**, 101.
3 X. Li, Y. Xie, B. Song, H. L. Zhang, H. Chen, H. Cai, W. Liu and Y. Tang, *Angew. Chem., Int. Ed.*, 2017, **56**, 2689.
4 P. Wei, X. Yan and F. Huang, *Chem. Soc. Rev.*, 2015, **44**, 815.
5 P. Chen, Q. Li, S. Grindy and N. Holten-Andersen, *J. Am. Chem. Soc.*, 2015, **137**, 11590.
6 S. Palagi and P. Fischer, *Nat. Rev. Mater.*, 2018, **3**, 113.
7 M. Irie, T. Fulcaminato, K. Matsuda and S. Kobatake, *Chem. Rev.*, 2014, **114**, 12174.
8 T. Mutai, H. Satou and K. Araki, *Nat. Mater.*, 2005, **4**, 685.
9 S. J. Yoon, J. W. Chung, J. Gierschner, K. S. Kim, M. G. Choi, D. Kim and S. Y. Park, *J. Am. Chem. Soc.*, 2010, **132**, 13675.
10 S. Inagi, H. Nagai, I. Tomita and T. Fuchigami, *Angew. Chem., Int. Ed.*, 2013, **52**, 6616.
11 C. M. Amb, A. L. Dyer and J. R. Reynolds, *Chem. Mater.*, 2011, **23**, 397.
12 A. B. Powell, C. W. Bielawski and A. H. Cowley, *J. Am. Chem. Soc.*, 2010, **132**, 10184.
13 Z. Qiu, W. Zhao, M. Cao, Y. Wang, J. W. Y. Lam, Z. Zhang, X. Chen and B. Z. Tang, *Adv. Mater.*, 2018, **30**, 1803924.
14 W. Zhao, Z. He, Q. Peng, J. W. Y. Lam, H. Ma, Z. Qiu, Y. Chen, Z. Zhao, Z. Shuai, Y. Dong and B. Z. Tang, *Nat. Commun.*, 2018, **9**, 1.
15 J. Li, H. K. Bisoyi, J. Tian, J. Guo and Q. Li, *Adv. Mater.*, 2019, **31**, 1807751.
16 T. Grotjohann, I. Testa, M. Leutenegger, H. Bock, N. T. Urban, F. Lavoie-Cardinal, K. I. Willig, C. Eggeling, S. Jakobs and S. W. Hell, *Nature*, 2011, **478**, 204.
17 F. P. G. de Arquer, A. Armin, P. Meredith and E. H. Sargent, *Nat. Rev. Mater.*, 2017, **2**, 1.
18 Z. Wu, C. Ji, X. Zhao, Y. Han, K. Mullen, K. Pan and M. Yin, *J. Am. Chem. Soc.*, 2019, **141**, 7385.
19 F. Li, X. Wang, Z. Xia, C. Pan and Q. Liu, *Adv. Funct. Mater.*, 2017, **27**, 1700051.
20 Z. Li, G. Wang, Y. Ye, B. Li, H. Li and B. Chen, *Angew. Chem., Int. Ed.*, 2019, **131**, 18193.
21 T. Bian, Z. Chu and R. Klajn, *Adv. Mater.*, 2020, **32**, 1905866.
22 X. Tang, Z. Huang, H. Chen, Y. Kang, J. F. Xu and X. Zhang, *Angew. Chem., Int. Ed.*, 2018, **57**, 8545.
23 Y. Fu, H. H. Han, J. Zhang, X. P. He, B. L. Feringa and H. Tian, *J. Am. Chem. Soc.*, 2018, **140**, 8671.
24 K. Iwaso, Y. Takashima and A. Harada, *Nat. Chem.*, 2016, **8**, 625.
25 B. R. Donovan, V. M. Matavulj, S. K. Ahn, T. Gain and T. J. White, *Adv. Mater.*, 2019, **31**, 1805750.
26 A. M. Rice, C. R. Martin, V. A. Galitskiy, A. A. Berseneva, G. A. Leith and N. B. Shustova, *Chem. Rev.*, 2020, **120**, 8790.
27 S. Garg, H. Schwartz, M. Kozlowska, A. B. Kanj, K. Muller, W. Wenzel, U. Ruschewitz and L. Heinke, *Angew. Chem., Int. Ed.*, 2019, **58**, 1193.
28 M. M. Lerch, W. Szymanski and B. Feringa, *Chem. Soc. Rev.*, 2018, **47**, 1910.
29 Z. Gao, Y. Han and F. Wang, *Nat. Commun.*, 2018, **9**, 1.
30 J. Hai, T. Li, J. Su, W. Liu, Y. Ju, B. Wang and Y. Hou, *Angew. Chem., Int. Ed.*, 2018, **57**, 6786.
31 Y. Yao, J. T. Waters, A. V. Shneidman, J. Cui, X. Wang, N. K. Mandsberg, S. Li, A. C. Balazs and J. Aizenberg, *Proc. Natl. Acad. Sci. U. S. A.*, 2018, **115**, 12950.
32 H. Sun, S. Liu, W. Lin, K. Y. Zhang, W. Lv, X. Huang, F. Huo, H. Yang, G. Jenkins, Q. Zhao and W. Huang, *Nat. Commun.*, 2014, **5**, 1.
33 M. Tu, H. Reinsch, S. Rodriguez-Hermida, R. Verbeke, T. Stassin, W. Egger, M. Dickmann, B. Dieu, J. Hofkens, I. F. J. Vankelecom, N. Stock and R. Ameloot, *Angew. Chem., Int. Ed.*, 2019, **131**, 2445.
34 P. Zijlstra, J. W. M. Chon and M. Gu, *Nature*, 2009, **459**, 410.
35 W. Zhao, Z. Liu, J. Yu, X. Lu, J. W. Y. Lam, J. Sun, Z. He, H. Ma and B. Z. Tang, *Adv. Mater.*, 2021, **33**, 2006844.
36 H. Dong, H. Zhu, Q. Meng, X. Gong and W. Hu, *Chem. Soc. Rev.*, 2012, **41**, 1754.
37 R. Pardo, M. Zayat and D. Levy, *Chem. Soc. Rev.*, 2011, **40**, 672.
38 H. N. Kim, Z. Guo, W. Zhu, J. Yoon and H. Tian, *Chem. Soc. Rev.*, 2011, **40**, 79.
39 Y. Zhu, Y. Lv, Y. Xiao, H. Sun, Q. Zhang and X. Hao, *J. Lumin.*, 2019, **215**, 116626.
40 X. Zhang, L. Hou and P. Samori, *Nat. Commun.*, 2016, **7**, 1.
41 E. Orgiu and P. Samori, *Adv. Mater.*, 2014, **26**, 1827.
42 K. Chen, S. Schuenemann, S. Song and H. Tueysuez, *Chem. Soc. Rev.*, 2018, **47**, 7045.
43 M. V. Kovalenko, L. Protesescu and M. I. Bodnarchuk, *Science*, 2017, **358**, 745.
44 Q. A. Akkerman, G. Raino, M. V. Kovalenko and L. Manna, *Nat. Mater.*, 2018, **17**, 394.
45 J. Shamsi, A. S. Urban, M. Imran, L. De Trizio and L. Manna, *Chem. Rev.*, 2019, **119**, 3296.
46 Y. Wei, Z. Cheng and J. Lin, *Chem. Soc. Rev.*, 2019, **48**, 310.
47 L. Protesescu, S. Yakunin, M. I. Bodnarchuk, F. Krieg, R. Caputo, C. H. Hendon, R. X. Yang, A. Walsh and M. V. Kovalenko, *Nano Lett.*, 2015, **15**, 3692.
48 G. Nedelcu, L. Protesescu, S. Yakunin, M. I. Bodnarchuk, M. J. Grotevent and M. V. Kovalenko, *Nano Lett.*, 2015, **15**, 5635.
49 Y. Zhang, D. Lu, M. Gao, M. Lai, J. Lin, T. Lei, Z. Lin, L. N. Quan and P. Yang, *Proc. Natl. Acad. Sci. U. S. A.*, 2019, **116**, 12648.
50 K. Sun, D. Tan, X. Fang, X. Xia, D. Lin, J. Song, Y. Lin, Z. Liu, M. Gu, Y. Yue and J. Qiu, *Science*, 2022, **375**, 307.
51 Q. A. Akkerman, V. D'Innocenzo, S. Accornero, A. Scarpellini, A. Petrozza, M. Prato and L. Manna, *J. Am. Chem. Soc.*, 2015, **137**, 10276.
52 N. Peimyoo, M. D. Barnes, J. D. Mehew, A. De Sanctis, I. Amit, J. Escolar, K. Anastasiou, A. P. Rooney, S. J. Haigh,

S. Russo, M. F. Craciun and F. Withers, *Sci. Adv.*, 2019, **5**, eaau0906.
53 Z. Zhao, Y. Dai, D. Liu, L. Zhou, S. Li, Z. L. Wang and J. Wang, *Nat. Commun.*, 2020, **11**, 1.
54 J. Schneider, M. Matsuoka, M. Takeuchi, J. Zhang, Y. Horiuchi, M. Anpo and D. W. Bahnemann, *Chem. Rev.*, 2014, **114**, 9919.
55 R. Asahi, T. Morikawa, T. Ohwaki, K. Aoki and Y. Taga, *Science*, 2001, **293**, 269.
56 M. R. Hoffmann, S. T. Martin, W. Y. Choi and D. W. Bahnemann, *Chem. Rev.*, 1995, **95**, 69.
57 C. He, J. Cheng, X. Zhang, M. Douthwaite, S. Pattisson and Z. Hao, *Chem. Rev.*, 2019, **119**, 4471.
58 M. Imran, V. Caligiuri, M. Wang, L. Goldoni, M. Prato, R. Krahne, L. De Trizio and L. Manna, *J. Am. Chem. Soc.*, 2018, **140**, 2656.
59 H. Hu, L. Wu, Y. Tan, Q. Zhong, M. Chen, Y. Qiu, D. Yang, B. Sun, Q. Zhang and Y. Yin, *J. Am. Chem. Soc.*, 2018, **140**, 406.
60 X. Zhang, X. Bai, H. Wu, X. Zhang, C. Sun, Y. Zhang, W. Zhang, W. Zheng, W. W. Yu and A. L. Rogach, *Angew. Chem., Int. Ed.*, 2018, **57**, 3337.
61 Q. Zhong, M. Cao, Y. Xu, P. Li, Y. Zhang, H. Hu, D. Yang, Y. Xu, L. Wang, Y. Li, X. Zhang and Q. Zhang, *Nano Lett.*, 2019, **19**, 4151.
62 K. J. Doyle, H. Tran, M. Baldoni-Olivencia, M. Karabulut and P. E. Hoggard, *Inorg. Chem.*, 2008, **47**, 7029.
63 J. Borisch, S. Pilkenton, M. L. Miller, D. Raftery and J. S. Francisco, *J. Phys. Chem. B*, 2004, **108**, 5640.
64 L. Sheps, A. C. Crowther, C. G. Elles and F. F. Crim, *J. Phys. Chem. A*, 2005, **109**, 4296.
65 N. Aristidou, C. Eames, I. Sanchez-Molina, X. Bu, J. Kosco, M. S. Islam and S. A. Haque, *Nat. Commun.*, 2017, **8**, 1.
66 L. Zhang and P. H. L. Sit, *J. Mater. Chem. A*, 2017, **5**, 9042.
67 Q. Chen, J. Wu, X. Ou, B. Huang, J. Almutlaq, A. A. Zhumekenov, X. Guan, S. Han, L. Liang, Z. Yi, J. Li, X. Xie, Y. Wang, Y. Li, D. Fan, D. B. L. Teh, A. H. All, O. F. Mohammed, O. M. Bakr, T. Wu, M. Bettinelli, H. Yang, W. Huang and X. Liu, *Nature*, 2018, **561**, 88.
68 Q. A. Akkerman, E. Bladt, U. Petralanda, Z. Dang, E. Sartori, D. Baranov, A. L. Abdelhady, I. Infante, S. Bals and L. Manna, *Chem. Mater.*, 2019, **31**, 2182.
69 H. Wu, Y. Chen, W. Zhang, M. S. Khan and Y. Chi, *ACS Appl. Nano Mater.*, 2021, **4**, 11791.